Extending Qualitative Reconstruction in Biharmonic Scattering from Full to Limited Data

General Ozochiawaeze[1] Isaac Harris[1] Peijun Li[2]

[1] Department of Mathematics, Purdue University
[2] Chinese Academy of Sciences

Graduate Student Analysis Seminar
March 2025

Overview

Physical Intuition: Flexural Waves in Plates

- Send a wave towards an unknown obstacle and measure the reflected wave.
- **Key question:** What can the reflected wave tell us about the obstacle's shape or properties?
- Flexural waves are bending waves traveling in thin elastic plates.
- Modeled by the biharmonic wave equation, which captures plate bending.
- When these waves hit a cavity (hole), they scatter.
- Measuring scattered waves helps identify hidden cavities.

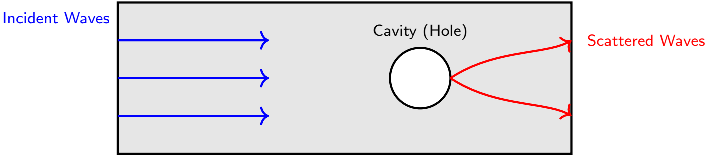

Thin Elastic Plate

Applications of Biharmonic Wave Scattering

- **Acoustic Black Hole:**
  - Used to control the propagation of sound waves, trapping them within a specific region.
- **Elastic Cloaking:**
  - Techniques to make objects undetectable to elastic waves, useful in vibration control.
- **Chladni Plate:**
  - The vibrating patterns formed on a plate under the influence of oscillations, representing modal shapes for Electronic Speckle Pattern Interferometry (ESPI).

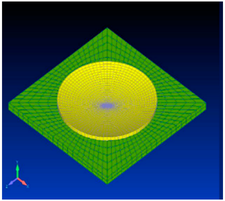

Figure: Acoustic Black Hole, American Society of Mechanical Engineers, 2015

Figure: Mechanical Cloaking for bridge support design structure

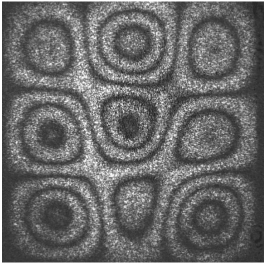

Figure: Chladni Plate for ESPI vibration modes

Biharmonic Clamped Scattering Problem

- Let $D \subset \mathbb{R}^2$ be a bounded domain such that $\mathbb{R}^2 \setminus \overline{D}$ is connected.
- The **total field** $u \in H^2_{\text{loc}}(\mathbb{R}^2 \setminus \overline{D})$ satisfies the **biharmonic wave equation**:

$$\Delta^2 u - \kappa^4 u = 0 \quad \text{in } \mathbb{R}^2 \setminus \overline{D}.$$

- **Clamped boundary conditions** on ∂D:

$$u = 0, \quad \partial_\nu u = 0 \quad \text{on } \partial D,$$

  where ∂_ν is the outward normal derivative.
- The total field decomposes as

$$u = u^i + u^s,$$

  where u^i is the incident flexural wave and u^s the scattered wave.
- Incident waves are **time-harmonic plane waves** of the form

$$u^i(x) = e^{i\kappa x \cdot d}, \quad d \in \mathbb{S}^1.$$

- The scattered field u^s satisfies the biharmonic Sommerfeld radiation condition:

$$\partial_r v - i\kappa v = O\left(r^{-\frac{3}{2}}\right) \quad \text{as } r \to \infty,$$

  where $v = u^s$ or Δu^s.

Decomposition of the Scattered Field

To analyze the biharmonic scattered field u^s, we introduce two auxiliary components that separate u^s into parts satisfying simpler equations:

$$\boxed{\begin{aligned} u^s_{\mathsf{H}} &:= -\frac{1}{2\kappa^2}\left(\Delta u^s - \kappa^2 u^s\right), \\ u^s_{\mathsf{M}} &:= \frac{1}{2\kappa^2}\left(\Delta u^s + \kappa^2 u^s\right), \end{aligned}}$$

where

$$u^s = u^s_{\mathsf{H}} + u^s_{\mathsf{M}}, \quad \Delta u^s = \kappa^2\left(u^s_{\mathsf{M}} - u^s_{\mathsf{H}}\right).$$

Here, u^s_{H} is called the **Helmholtz component**, since it satisfies the Helmholtz equation, while u^s_{M} is the **modified (anti-Helmholtz) component**, satisfying a modified Helmholtz equation:

$$\begin{cases} \Delta u^s_{\mathsf{H}} + \kappa^2 u^s_{\mathsf{H}} = 0, \\ \Delta u^s_{\mathsf{M}} - \kappa^2 u^s_{\mathsf{M}} = 0, \end{cases} \qquad \text{in } \mathbb{R}^2 \setminus \overline{D}.$$

This decomposition allows us to study u^s via two second-order PDEs instead of a single fourth-order equation.

Coupled Scattering Problem

The original biharmonic scattering problem can be reformulated as a coupled system for the Helmholtz and modified Helmholtz components:

$$\begin{cases} \Delta u_{\mathsf{H}}^s + \kappa^2 u_{\mathsf{H}}^s = 0, \\ \Delta u_{\mathsf{M}}^s - \kappa^2 u_{\mathsf{M}}^s = 0, \end{cases} \qquad \text{in } \mathbb{R}^2 \setminus \overline{D},$$

with coupled boundary conditions on ∂D:

$$u_{\mathsf{H}}^s + u_{\mathsf{M}}^s = -u^i, \quad \partial_\nu u_{\mathsf{H}}^s + \partial_\nu u_{\mathsf{M}}^s = -\partial_\nu u^i,$$

and radiation conditions as $r = |x| \to \infty$:

$$\lim_{r\to\infty} \sqrt{r}\,(\partial_r u_{\mathsf{H}}^s - i\kappa u_{\mathsf{H}}^s) = 0, \quad \lim_{r\to\infty} \sqrt{r}\,(\partial_r u_{\mathsf{M}}^s - i\kappa u_{\mathsf{M}}^s) = 0.$$

Asymptotic behavior:

$$|u_{\mathsf{H}}^s| = \mathcal{O}\left(\frac{1}{\sqrt{r}}\right), \quad |u_{\mathsf{M}}^s| = \mathcal{O}\left(\frac{e^{-\kappa r}}{\sqrt{r}}\right),$$

which follows from their Fourier-Hankel expansions and Bessel function asymptotics.

Coupled Scattering Problem

The original biharmonic scattering problem can be reformulated as a coupled system for the Helmholtz and modified Helmholtz components:

$$\begin{cases} \Delta u_{\mathsf{H}}^s + \kappa^2 u_{\mathsf{H}}^s = 0, \\ \Delta u_{\mathsf{M}}^s - \kappa^2 u_{\mathsf{M}}^s = 0, \end{cases} \qquad \text{in } \mathbb{R}^2 \setminus \overline{D},$$

with coupled boundary conditions on ∂D:

$$u_{\mathsf{H}}^s + u_{\mathsf{M}}^s = -u^i, \quad \partial_\nu u_{\mathsf{H}}^s + \partial_\nu u_{\mathsf{M}}^s = -\partial_\nu u^i,$$

and radiation conditions as $r = |x| \to \infty$:

$$\lim_{r\to\infty} \sqrt{r}\,(\partial_r u_{\mathsf{H}}^s - i\kappa u_{\mathsf{H}}^s) = 0, \quad \lim_{r\to\infty} \sqrt{r}\,(\partial_r u_{\mathsf{M}}^s - i\kappa u_{\mathsf{M}}^s) = 0.$$

Asymptotic behavior:

$$|u_{\mathsf{H}}^s| = \mathcal{O}\left(\frac{1}{\sqrt{r}}\right), \quad |u_{\mathsf{M}}^s| = \mathcal{O}\left(\frac{e^{-\kappa r}}{\sqrt{r}}\right),$$

which follows from their Fourier-Hankel expansions and Bessel function asymptotics.
Key advantage: The anti-Helmholtz component u_{M}^s decays *exponentially* at infinity, which greatly simplifies analysis and numerical treatment!

Fundamental Solution and Green's Representation

Fundamental Solutions of Helmholtz-type Equations
Let $\Phi_\kappa(x)$ and $\Phi_{i\kappa}(x)$ be the fundamental solutions in $\mathbb{R}^2$ of:

$$(\Delta + \kappa^2)\Phi_\kappa(x) = -\delta(x), \quad (\Delta - \kappa^2)\Phi_{i\kappa}(x) = -\delta(x)$$

Then: Fundamental Solution of Biharmonic Wave Operator

$$G_\kappa(x) = \frac{1}{2\kappa^2}\left(\Phi_{i\kappa}(x) - \Phi_\kappa(x)\right), \quad (\Delta^2 - \kappa^4)G_\kappa(x) = -\delta(x)$$

Green's Representation for the Scattered Field
The scattered field u^s satisfies:

$$\begin{aligned} u^s(x) &= \int_{\partial D} \left[\partial_\nu u^s(y)\, G_\kappa(x-y) - u^s(y)\, \partial_\nu G_\kappa(x-y)\right] ds(y) \\ &= \int_{\partial D} \left[\partial_\nu u^s(y)\, \Phi_\kappa(x-y) - u^s(y)\, \partial_\nu \Phi_\kappa(x-y)\right] ds(y) \end{aligned}$$

Note: The fundamental solution for the 2D (anti-) Helmholtz equation is given by

$$\Phi_\kappa(x) = \frac{i}{4} H_0^{(1)}(\kappa|x|), \quad \Phi_{i\kappa}(x) = \frac{i}{4} H_0^{(1)}(i\kappa|x|),$$

where $H_0^{(1)}$ is the Hankel function of the first kind of order zero.

Far-Field Behavior and the Inverse Problem (Biharmonic)

We recall the fundamental solution of the 2D biharmonic wave operator:

$$G_\kappa(x-y) = \frac{1}{2\kappa^2}\left[\Phi_{i\kappa}(x-y) - \Phi_\kappa(x-y)\right]$$

Far-Field Expansion:

$$\Phi_\kappa(x-y) = \frac{i}{4}H_0^{(1)}(\kappa|x-y|) \sim \frac{e^{i\kappa|x|}}{\sqrt{|x|}}\, e^{-i\kappa\hat{x}\cdot y}, \quad \text{as } |x| \to \infty$$

Hence,

$$G_\kappa(x-y) \sim -\frac{1}{2\kappa^2}\cdot\frac{e^{i\kappa|x|}}{\sqrt{|x|}}\, e^{-i\kappa\hat{x}\cdot y} \quad \text{since } \Phi_{i\kappa} \text{ decays exponentially.}$$

Substituting into Green's representation yields the far-field expansion:

$$u^s(x) = \frac{e^{i\kappa|x|}}{\sqrt{|x|}}u^\infty(\hat{x}) + \mathcal{O}(|x|^{-3/2}), \quad \hat{x} = \frac{x}{|x|}$$

Far-Field Pattern:

$$u^\infty(\hat{x}) := -\frac{1}{2\kappa^2\sqrt{8\pi\kappa}}\int_{\partial D}\left[\partial_\nu u^s(y)e^{-i\kappa\hat{x}\cdot y} - u^s(y)\partial_\nu e^{-i\kappa\hat{x}\cdot y}\right] ds(y)$$

Inverse Problem: Given $u^\infty(\hat{x})$ for all $\hat{x}$ for one or more incident waves, reconstruct the unknown cavity $D \subset \mathbb{R}^2$.

Sampling Methods

Examples of sampling methods. *Linear Sampling Method* (Colton-Kirsch, 1996), *Factorization Method* (Kirsch 1998), *Probe Method* (Potthast, 2001), *Reciprocity Gap Method* (Colton-Haddar, 2005),...)

Principle: the idea is to construct an indicator test function $\mathcal{I}(z)$ that will test whether a sampling point z is in the interior or exterior of the scatterer (i.e. $\mathcal{I}(z) \approx 1$ inside scatterer, $\mathcal{I}(z) \approx 0$ outside scatterer).

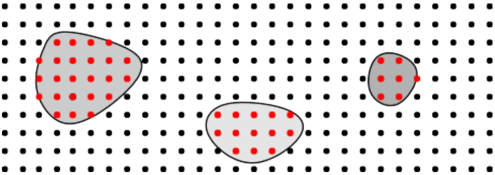

(+) Non-iterative, the computation of $\mathcal{I}$ does not require a forward solver.
(-) Requires a large amount of multi-static data (many transmitters-receivers).

Linear Sampling Method (LSM) — Core Idea

Goal: Determine whether a sampling point $z \in \mathbb{R}^2$ lies inside the unknown cavity $D \subset \mathbb{R}^2$.

LSM Equation:

$$\mathcal{F} g_z = G_\kappa^\infty(\cdot, z), \quad (\mathcal{F} g_z)(\hat{x}) := \int_{\mathbb{S}^1} u^\infty(\hat{x}, d)\, g_z(d)\, ds(d)$$

Where:

- $\mathcal{F}$: Far-field operator mapping weights g_z to superpositions of measured data.
- $G_\kappa^\infty(\cdot, z)$: Far-field pattern of a biharmonic point source at z.

Sampling Principle:

- *Feasible* (regularized) solutions g_z exist with small norm if and only if $z \in D$.
- *Indicator:* Plotting $\|g_z\|_{L^2}$ reveals the support of D.

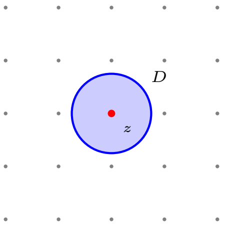

Ill-posedness and Approximate Solvability in LSM

Issue: The LSM equation

$$\mathcal{F} g_z = G_\kappa^\infty(\cdot, z)$$

is ill-posed because the far-field operator $\mathcal{F} \colon L^2(\mathbb{S}^1) \to L^2(\mathbb{S}^1)$ is **compact**.

Why? The kernel $u^\infty(\hat{x}, d)$ of $\mathcal{F}$ is *analytic* in both variables $(\hat{x}, d) \in \mathbb{S}^1 \times \mathbb{S}^1$, leading to smoothing behavior and thus compactness.

Approximate Solvability Condition (Key Property)

For the LSM to function as a reliable indicator method, we want:

$\mathcal{F}$ is injective with dense range in $L^2(\mathbb{S}^1)$.

This allows us to use regularized solutions g_z to test membership of $z \in D$.

Interpretation: While exact solutions g_z may not exist, we can seek *approximate* solutions whose norms reveal geometric information about the scatterer.

Injectivity via Clamped Transmission Problem

Assume: $\mathcal{F}g = u_g^\infty = 0 \Rightarrow u_g^\infty = 0, \quad u_g = u_g^s + v_g, \quad v_g(x) = \int_{\mathbb{S}^1} e^{i\kappa x\cdot d} g(d)\, ds(d)$

Step 1: $u_g^\infty = 0$ implies $u_{\mathsf{H},g}^s = 0$ in $\mathbb{R}^2 \setminus \overline{D}$ (Rellich's lemma)

Step 2: On ∂D, we have from the total field continuity:

$$v_g + u_{\mathsf{M},g}^s = 0, \quad \text{on } \partial D$$

Let:

$$q := u_{\mathsf{H},g} = v_g \quad \text{(incident Herglotz field)}, \quad p := u_{\mathsf{M},g}^s \quad \text{(scattered field)}$$

Then $q + p = 0$ and $\partial_\nu q + \partial_\nu p = 0$ on ∂D, so:

Clamped Transmission Problem:

$$\begin{cases} (\Delta - \kappa^2)p = 0 \text{ in } \mathbb{R}^2 \setminus \overline{D}, \quad (\Delta + \kappa^2)q = 0 \text{ in } D, \\ q + p = 0, \quad \partial_\nu q + \partial_\nu p = 0 \text{ on } \partial D. \end{cases}$$

Conclusion

If the only solution to this problem is $q = p = 0$, so κ^2 is **NOT** a clamped eigenvalue, then $\mathcal{F}$ is injective.

Reciprocity and Dense Range of $\mathcal{F}$

Reciprocity Relation (Biharmonic Far-Field):

$$u^\infty(\hat{x}, d) = u^\infty(-d, -\hat{x})$$

(Follows from Green's representation for far-field pattern and exponential decay of anti-Helmholtz component.)

Adjoint Relationship: The reciprocity identity implies:

$$(\mathcal{F}^*\varphi)(d) = \int_{\mathbb{S}^1} u^\infty(-d, -\hat{x})\, \varphi(\hat{x})\, ds(\hat{x}) = (\mathcal{F}\tilde{\varphi})(d), \quad \text{where } \tilde{\varphi}(\hat{y}) = \varphi(-\hat{y})$$

Conclusion: $\mathcal{F}^*$ shares the same range properties as $\mathcal{F}$, hence:

Theorem (Injectivity and Density of $\mathcal{F}$)

Assume κ^2 is not a clamped eigenvalue of the clamped transmission problem. Then the far-field operator

$$\mathcal{F} : L^2(\mathbb{S}^1) \to L^2(\mathbb{S}^1)$$

is injective and has dense range.

Operator Factorization and Range Test Property

We factor the far-field operator as:

$$\mathcal{F} = \mathcal{G} \circ (-\mathcal{H}),$$

where

- $\mathcal{H}g = (v_g|_{\partial D}, \partial_\nu v_g|_{\partial D}), \quad v_g(x) = \int_{\mathbb{S}^1} g(d) e^{i\kappa x \cdot d}\, ds(d)$ is the Herglotz wave function.
  Maps: $L^2(\mathbb{S}^1) \to H^{3/2}(\partial D) \times H^{1/2}(\partial D)$.
- $\mathcal{G}(h_1, h_2) = w^\infty$, where w solves:

$$\begin{cases} \Delta^2 w - \kappa^4 w = 0 & \text{in } \mathbb{R}^2 \setminus \overline{D}, \\ w = h_1, \quad \partial_\nu w = h_2 & \text{on } \partial D, \\ w, \Delta w \text{ satisfy Sommerfeld radiation condition.} \end{cases}$$

  Maps: $H^{3/2}(\partial D) \times H^{1/2}(\partial D) \to L^2(\mathbb{S}^1)$.

Range Test Property: $z \in D \iff G_\kappa^\infty(\cdot, z) \in \text{Range}(\mathcal{G})$

Significance: Although the far-field equation $\mathcal{F}g = G_\kappa^\infty(\cdot, z)$ is generally not exactly solvable, it is **approximately solvable** in a regularized sense if and only if $z \in D$. The norm of regularized solutions g_z is **small** precisely when the sampling point z is inside the scatterer.

Theoretical Justification for the LSM Indicator

Theorem

Assume κ^2 is not a transmission eigenvalue for the clamped biharmonic problem. Then for each sampling point $z \in \mathbb{R}^2$, consider the regularized equation The behavior of $\|g_z^\alpha\|_{L^2(\mathbb{S}^1)}$ distinguishes the location of z as follows:

(i) *If $z \in D$, then there exists a sequence of regularized solutions g_z^α such that*

$$\lim_{\alpha \to 0} ||\mathcal{F} g_z^\alpha - G_\kappa^\infty(\cdot, z)||_{L^2(\mathbb{S}^1)} = 0, \quad \textit{and} \quad \lim_{z \to \partial D} \|g_z^\alpha\|_{L^2(\mathbb{S}^1)} = \infty.$$

(ii) *If $z \notin D$, then for any such sequence, the norms diverge:*

$$\lim_{\alpha \to 0} \|g_z^\alpha\|_{L^2} = \infty.$$

Interpretation: Indicator $\mathcal{I}(z) := 1/||g_z^\alpha||_{L^2}$.

- If $z \notin D$, then $\|g_z^\alpha\|_{L^2} \to \infty$ as $\alpha \to 0$, so $I(z) \to 0$.
- If $z \in D$, then $\|g_z^\alpha\|_{L^2}$ remains bounded, so $I(z) > 0$.

Algorithmic Aspects

- A regularization is needed to solve the far-field equation, e.g., we used Tikhonov reg. with $\alpha = 10^{-6}$ in all reconstructions

$$(\alpha I + F_d^* F_d) g_z^\alpha = F_d^* \phi_z$$

- Dimension of discretized matrix is based on the number N of sources/receivers. We selected a 250-by-250 grid for each construction.

  Example: 30 sources/receivers yields a 30-by-30 matrix F_d

- $F_d = [u^\infty(\hat{x}_i, \hat{y}_j)]_{i,j=1}^d$. Discretize so that

$$\hat{x}_i = \hat{y}_j = (\cos\theta_i, \sin\theta_j), \quad \theta_i = 2\pi(i-1)/d, \; i = 1, \dots, d.$$

  We used Li and Dong's boundary integral equation method to approximate the discretized far-field operator F_d.

- Add noise to test the stability of the LSM

$$F_d^\delta = [F_{i,j}(1 + \delta E_{i,j})]_{i,j=1}^d, \quad ||E||_2 = 1.$$

  $E \in \mathbb{C}^{d \times d}$ is a matrix with random entries, $0 < \delta \ll 1$ relative noise level

Numerical Result: Recovering the Apple-Shaped Cavity

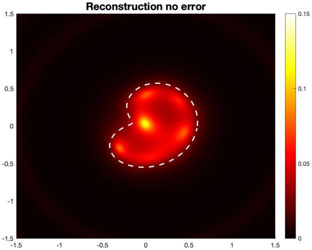

Figure: Recovering the Apple-Shaped Cavity with $\kappa = 2\pi$; no noise; 30 incident and observation directions; 250×250 grid

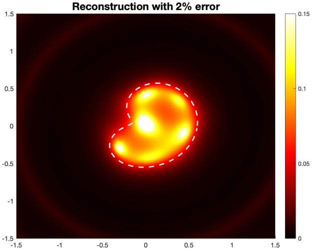

Figure: Recovering the Apple-Shaped Cavity with $\kappa = 2\pi$; noise $\delta = 0.02$; 30 incident and observation directions; 250×250 grid

Parametrization of Apple. $\gamma(t) = \frac{0.55(1+0.9\cos t+0.1\sin 2t}{1+0.75\cos t}(\cos t, \sin t)$

Numerical Result: Recovering the $\partial D \in C^2$ Peach-Shaped Cavity

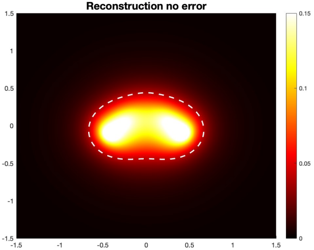

Figure: Recovering the Peach-Shaped Cavity with $\kappa = \pi$; no noise; 30 incident and observation directions; 250×250 grid

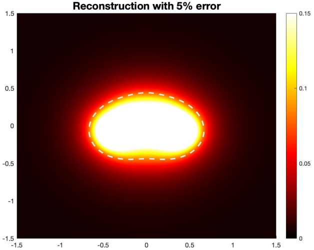

Figure: Recovering the Peach-Shaped Cavity with $\kappa = \pi$; noise $\delta = 0.05$; 30 incident and observation directions; 250×250 grid

Parametrization of Peach. $\gamma(t) = 0.22(\cos^2 t\sqrt{1-\sin t} + 2)(\cos t, \sin t)$

Extended Sampling Method

Extended Sampling Method for Far-Field Measurement

- Helmholtz equation: Applied in various works:
  - Juan Liu, Jiguang Sun (2018) – One-wave data
  - Li, Deng, & Sun (2020) – Bayesian method for limited aperture
  - Fang Zeng (2020) – Interior inverse scattering
  - Sun & Zhang (2023) – Inverse source/multifrequency data
- Elastic wave equation: Liu, J., Liu, X., & Sun (2019) – One-wave data

Why Extended Sampling?

- Versatile: Works with one-wave, multi-wave, and multifrequency data.
- Effective with limited data.

This talk: Applying this method to the biharmonic wave equation with one-wave and multifrequency data.

Key Equation: The indicator function $\mathcal{I}(z) := ||g_z||_{L^2(S^1)}$ comes from solving for the weight function $g = g_z$:

$$\underbrace{(\mathcal{F}_{B_z} g)(\hat{x})}_{\text{Superposition of shifted ball's far-field data}} = \underbrace{u^\infty(\hat{x})}_{\text{Measured biharmonic far-field data}} \quad \text{for a } \textbf{single} \text{ incident wave } d.$$

Indicator Function Behavior

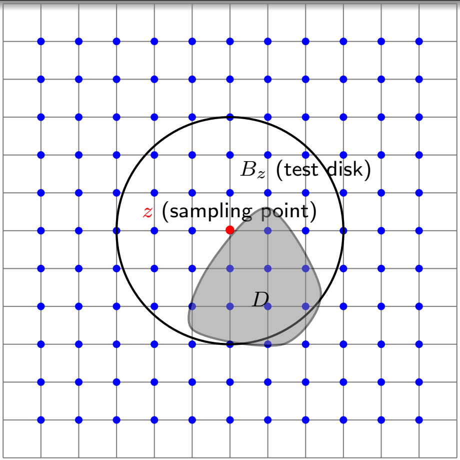

$\mathcal{I}(z) := ||g_z||_{L^2(S^1)}$ will take large values if $D \cap B_z = \emptyset$

$\mathcal{I}(z) := ||g_z||_{L^2(S^1)}$ will take small values if $D \subsetneq B_z$

Extended Sampling Method: Scattering Problem

Let $B_z = B(z, R)$ be a sound-soft disk centered at sampling point $z \subset \mathbb{R}^2$. Define $U_{B_z}(x, \hat{y})$ as the solution of:

$$\begin{cases} \Delta U_{B_z} + \kappa^2 U_{B_z} = 0 & \text{in } \mathbb{R}^2 \setminus \overline{B_z}, \\ U_{B_z} = -e^{i\kappa x \cdot \hat{y}} & \text{on } \partial B_z, \\ \lim\limits_{r \to \infty} \sqrt{r}\,(\partial_r U_{B_z} - i\kappa U_{B_z}) = 0 & \end{cases}$$

The far-field pattern $U^{\infty}_{B_z}(\hat{x}, \hat{y})$ satisfies:

$$U^{\infty}_{B_z}(\hat{x}, \hat{y}) = e^{i\kappa z \cdot (\hat{y} - \hat{x})} U^{\infty}_{B_0}(\hat{x}, \hat{y})$$

Main Benefit: Closed-form expression for the far-field pattern of the *unshifted*

sound-soft disk $B_0 = B(0, R)$:

$$U^{\infty}_{B_0}(\hat{x}, \hat{y}) = -\frac{e^{-i\pi/4}}{\sqrt{2\pi\kappa}} \left[J_0(\kappa R) \frac{1}{H^{(1)}_0(\kappa R)} + 2 \sum_{n=1}^{\infty} J_n(\kappa R) \frac{\cos(n\theta)}{H^{(1)}_n(\kappa R)} \right]$$

where θ is the angle between $\hat{x}$ and $\hat{y}$.

Use: Enables efficient evaluation of $U^{\infty}_{B_z}$ via translation.

Extended Sampling Method Far-Field Equation

Define the operator

$$\mathcal{F}_{B_z} : L^2(\mathbb{S}^1) \to L^2(\mathbb{S}^1), \quad (\mathcal{F}_{B_z} g_z)(\hat{x}) = \int_{\mathbb{S}^1} U^\infty_{B_z}(\hat{x}, \hat{y})\, g_z(\hat{y})\, ds(\hat{y}).$$

(ESM Far-Field Equation)

$$\boxed{\mathcal{F}_{B_z} g_z = u^\infty, \quad \hat{x} \in \mathbb{S}^1}$$

Idea: For each sampling point z, solve the above equation for g_z. If a solution exists, it suggests the unknown cavity $D \subseteq B_z$.

Key Challenge: This equation is ill-posed since $\mathcal{F}_{B_z}$ is a compact operator with an analytic kernel.

Motivation: This motivates introducing auxiliary operators and regularization techniques to effectively solve the inverse problem.

Auxiliary Operators and Their Properties

Define two key operators associated with the test disk B_z:

- $\mathcal{G}_{B_z} : H^{1/2}(\partial B_z) \to L^2(\mathbb{S}^1)$ maps Dirichlet boundary data f to the far-field pattern V^∞ of the radiating solution V solving

$$\begin{cases} \Delta V + \kappa^2 V = 0, & \text{in } \mathbb{R}^2 \setminus \overline{B}_z, \\ V = f, & \text{on } \partial B_z, \\ \text{Sommerfeld radiation condition at } \infty. \end{cases}$$

- $\mathcal{H}_{B_z} : L^2(\mathbb{S}^1) \to H^{1/2}(\partial B_z)$ maps g to the boundary trace of the Herglotz wave function

$$v_g(x) = \int_{\mathbb{S}^1} g(\hat{y}) e^{i\kappa x \cdot \hat{y}} ds(\hat{y}), \quad x \in \partial B_z.$$

The far-field operator factorizes as

$$\mathcal{F}_{B_z} = \mathcal{G}_{B_z} \circ (-\mathcal{H}_{B_z}).$$

Key properties:

- If κ^2 is not a Dirichlet eigenvalue on B_z, then $\mathcal{H}_{B_z}$ is injective with dense range.
- $\mathcal{G}_{B_z}$ is injective and has dense range.
- Consequently, $\mathcal{F}_{B_z}$ is injective with dense range.
- All these operators are compact.

Main Theorem for ESM

Theorem

Let B_z be a disk centered at a sampling point z with radius R, and let D be a cavity in a thin plate with clamped boundary conditions. Assume that κ^2 is not a Dirichlet eigenvalue of $-\Delta$ in B_z. Then, the following hold for the modified far-field equation:

1. *If $D \subset B_z$, then for any $\epsilon > 0$, there exists a function $g_z^\alpha \in L^2(\mathbb{S}^1)$ such that*

$$||\mathcal{F}_{B_z} g_z^\alpha - u^\infty(\hat{x})_{L^2(\mathbb{S}^1)}|| \leq \epsilon. \qquad (1)$$

Moreover, the associated Herglotz wave function

$$v_{g_z^\alpha}(x) := \int_{\mathbb{S}^1} e^{i\kappa x\cdot d} g_z^\alpha(d)\, ds(d), \quad x \in B_z,$$

converges to the solution v of the Helmholtz equation in B_z with

$$v = -u_H^s \quad \text{on } \partial B_z$$

as $\alpha \to 0$.

2. *If $D \cap B_z = \emptyset$, then for every g_z^α satisfying (1) with a given $\epsilon > 0$, we have*

$$\lim_{\alpha\to 0} ||g_z^\alpha||_{L^2(\mathbb{S}^1)} = \infty.$$

Multilevel Extended Sampling Method (ESM) Algorithm Overview

1. **Initial Sampling:**
   - Choose a large radius R.
   - Generate a sampling grid T with points spaced roughly R apart.
   - Use ESM to find the global minimum point $z_0 \in T$ of $\|g_z^\alpha\|_{L^2}$.
   - Set D_0 as an initial approximation of the cavity D.
2. **Refinement Loop (for $j = 1, 2, \ldots$):**
   - Set finer radius $R_j = \frac{R}{2^j}$.
   - Generate a finer sampling grid T_j with points spaced roughly R_j.
   - Find the minimum point $z_j \in T_j$.
   - If $z_j \notin D_{j-1}$, stop and go to Step 3.
3. **Final Output:**

$$z_{j-1}, \quad D_{j-1} \quad \text{as the estimated location and shape of } D.$$

This multilevel strategy improves accuracy by zooming in progressively on the cavity location.

Numerical Simulation: Multilevel ESM

- **Method**: Multilevel Extended Sampling Method (MESM) used for numerical simulation – multilevel iteratively selects best radius
- **Objective**: Simulate scattering from apple-shaped cavities using varying positions.
- **Subfigures**:
  - **Apple cavity at origin** - Simulation for a cavity centered at the origin.
  - **Apple cavity at (-1.5, 1.5)** - Simulation for a cavity shifted to the position (-1.5, 1.5).
  - **Incident direction** $d = (1/2, \sqrt{3}/2)$ (fixed).

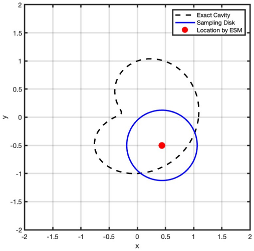

Figure: Apple cavity at origin

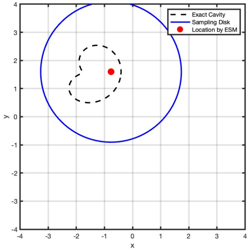

Figure: Apple cavity at (-1.5, 1.5)

Numerical Simulation: Multilevel ESM

- **Method**: Multilevel Extended Sampling Method (MESM) used for numerical simulation – multilevel iteratively selects best radius
- **Objective**: Simulate scattering from peach-shaped cavities using varying positions.
- **Subfigures**:
  - **Peach cavity at origin** - Simulation for a cavity centered at the origin.
  - **Peach cavity at (-1.5, 1.5)** - Simulation for a cavity shifted to the position (-1.5, 1.5).
  - **Incident direction** $d = (1/2, \sqrt{3}/2)$ (fixed).

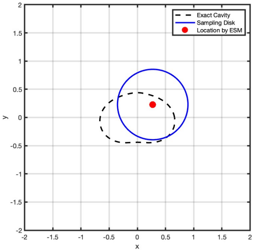

Figure: Peach cavity at origin

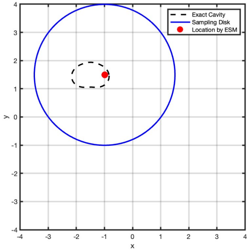

Figure: Peach cavity at (-1.5, 1.5)

Multi-Incident Direction ESM: Peach Cavity

- **Objective**: Simulate scattering from a peach-shaped cavity at a fixed frequency. Benefit: no need to find best radius R.
- **Input Data**:
  - $u^{\infty}(\hat{x_i}, d_j, \kappa)$: Far-field data for multiple incident directions d_j at fixed frequency 2π.
  - Incident apertures referring to each d_j:

$$\gamma_2^i = \left\{ (\cos\theta, \sin\theta) \mid \theta \in \left\{ 0, \frac{\pi}{8}, \frac{\pi}{4}, \frac{3\pi}{8}, \frac{\pi}{2} \right\} \right\}$$

$$\gamma_3^i = \left\{ (\cos\theta, \sin\theta) \mid \theta \in \left\{ 0, \frac{\pi}{5}, \frac{2\pi}{5}, \frac{3\pi}{5}, \frac{4\pi}{5}, \pi, \frac{6\pi}{5}, \frac{7\pi}{5}, \frac{8\pi}{5}, \frac{9\pi}{5} \right\} \right\}$$

  - Radius $R = 1$ (fixed)

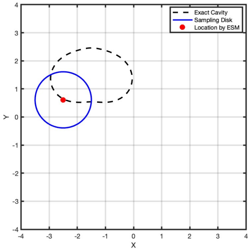

Figure: Peach cavity from γ_1^i

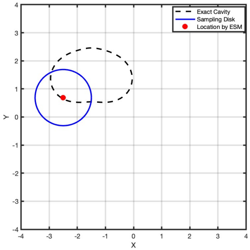

Figure: Peach cavity from γ_2^i

Multifrequency ESM: Peach Cavity

- **Objective**: Simulate scattering from a peach-shaped cavity across multiple frequencies. Benefit: no need to find best radius R
- **Frequency Range**:

$$[\kappa_{\min}, \kappa_{\max}] = \begin{cases} [\pi, 2\pi] & \text{(first frequency range)} \\ [\frac{\pi}{3}, 5\pi] & \text{(second frequency range)} \end{cases}$$

- **Input Data**:
  - $u^{\infty}(\hat{x}_i, d, \kappa_\ell)$: Far-field data for various incident directions and frequencies.
  - Incident direction $d = (1/2, \sqrt{3}/2)$ (fixed). Radius $R = 1$ (fixed)
  - Frequencies: κ_ℓ chosen at 5 distinct frequencies within the specified range.

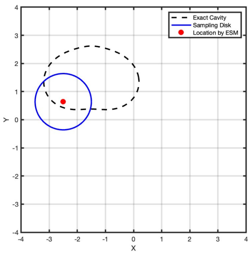

Figure: Peach cavity with range $[\pi, 2\pi]$

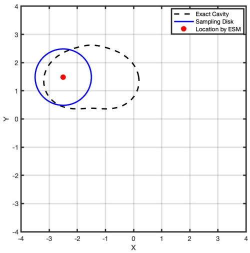

Figure: Peach cavity with range $[\frac{\pi}{3}, 5\pi]$

LSM vs. ESM — Key Differences

Data Requirements:

- LSM requires full multistatic far-field matrix (many incident directions).
- ESM works with limited-aperture or even single-direction data.

Computation:

- LSM involves solving ill-posed linear systems for each z.
- ESM reduces to simpler integral equations using known test disks.

Interpretation:

- LSM uses point-source test functions.
- ESM uses closed-form fields from known scatterers.

Conclusion: LSM is classical and complete, but ESM is more practical under data constraints.